



## STRUCTURAL, IMPEDANCE SPECTROSCOPIC AND CYCLIC VOLTAMMETRIC INVESTIGATIONS ON BIPBVOX SOLID ELECTROLYTE SYNTHESIZED BY ETHYLENE GLYCOL– CITRIC ACID SOL– GEL ROUTE

Elyas Sadeq AlAghbari<sup>1</sup>, Hakim Qaid Naji Museed Alarique<sup>2</sup>, Adel Qassem Saeed Shamsan<sup>2</sup>, Sameh A.S. Alariqi<sup>1</sup>, Niyazi Abdulmawla Sallam Al-Areqi<sup>1</sup>, Saba Beg<sup>3</sup>, Farea Naqvi<sup>3</sup>

<sup>1</sup>Department of Chemistry, Faculty of Applied Sciences, Taiz University, Taiz, Yemen.

<sup>2</sup>Department of Chemistry, Faculty of Education, Taiz University, Taiz, Yemen.

<sup>3</sup>Laboratory of Solid State Chemistry, Department of Chemistry, Aligarh Muslim University (AMU), Aligarh, India (202002).

### ABSTRACT

*Samples of BIPBVOX.x (Bi<sub>2</sub>V<sub>1-x</sub>Pb<sub>x</sub>O<sub>5.5-x/2</sub>) singly substituted system in the composition range 0.05 ≤ x ≤ 0.20 were prepared by ethylene glycol– citric acid sol–gel synthesis route. Structural investigations were carried out by using a combination of powder X–ray diffraction, FT–IR and DTA technique. The solid solutions with composition x ≤ 0.07 undergo α ↔ β phase transition, at 329°C and β ↔ γ phase transition at 419°C. The highly conducting γ'– phase was effectively stabilized at room temperature for compositions with x ≥ 0.17 whose thermal stability increases with Pb content. AC impedance spectra revealed that the conductivity is mainly due to the grain contribution to oxide– ion conductivity. At 300°C the highest value of conductivity (6.234 × 10<sup>-5</sup> S.cm<sup>-1</sup>) was obtained for composition x=0.15, while the highest value of conductivity at 600 °C (0.65 Scm<sup>-1</sup>) was observed for x=0.17. Cyclic voltammetric measurements showed reversible redox reactions of vanadium and irreversible redox reaction of Bi<sup>3+</sup> in the BIPBVOX system during the first cathodic and anodic sweep. However, a higher stability against the reduction of Bi<sup>3+</sup> to metallic bismuth was seen for x=0.20.*

**Keywords:** BIMEVOX; Phase transitions; AC impedance; Voltammetry.

## 1. Introduction

$\text{Bi}_4\text{V}_2\text{O}_{11}$  is a member of the Aurivillius family which can be viewed as an intergrowth of alternating  $(\text{VO}_{3.5}\square_{0.5})^{2-}$  anion deficient perovskite vanadate layers and  $(\text{Bi}_2\text{O}_2)^{2+}$  layers when the c-axis is traversed, where  $\square$  represents an oxide-ion vacancy. The high temperature phase,  $\gamma\text{-Bi}_4\text{V}_2\text{O}_{11}$ , has a good ionic conductivity above and crystallizes in the tetragonal  $I4/mmm$  space group with the a-axis dimension close to that of the perovskite,  $a \sim 3.90 \text{ \AA}$  [1,2]. The oxide-ion conductors known as BIMEVOXes, which are based on the cation substitution of vanadium in  $\text{Bi}_4\text{V}_2\text{O}_{11}$  constitute a recently discovered family of materials with very high oxide-ion conductivity [3–8]. The disordering of oxide-ion vacancies in the perovskite vanadate layers as a result of substitution of vanadium with aliovalent cations is responsible for the stabilization of  $\gamma$ -phase to room temperature.

Because of its best known conductivity at lower temperatures (e.g.,  $2 \times 10^{-3} \text{ S.cm}^{-1}$  at  $300^\circ\text{C}$ ) [2], The BICUVOX.10 ( $\text{Bi}_2\text{V}_{0.9}\text{Cu}_{0.1}\text{O}_{5.35}$ ) has been received much attention by several studies that have been devoted to investigate its oxide-ion performance by AC impedance spectroscopic measurements [9–11] and determine its redox stability limit by means of cyclic voltammetry [12–15]. In the literature survey, only one research work presented by Yan and Greenblatt [16] has reported detailed investigations on the compositional dependence of phase transitions and electrical conductivity of BIPBVOX. $x$  ( $\text{Bi}_2\text{V}_{1-x}\text{Pb}_x\text{O}_{5.5-x/2}$ ) synthesized by the solid synthesis route. However, the AC impedance spectroscopic and voltammetric investigations on this electrolyte system have never been reported yet. In the present paper, samples of BIPBVOX. $x$  ( $\text{Bi}_2\text{V}_{1-x}\text{Pb}_x\text{O}_{5.5-x/2}$ ;  $0.05 \leq x \leq 0.20$ ) were synthesized by ethylene glycol–citric acid route. The structural characterization was performed using X-ray powder diffraction (XRPD), FT-IR spectroscopy and Differential thermal analysis (DTA). The electrical properties were deduced from AC impedance spectra and cyclic voltammetry was used for the study of the redox stability of saturated  $\gamma$ -BIPBVOX solid solutions.

## 2. Experimental

### 2.1. Synthesis procedure

Solid solutions of the BIPBVOX. $x$  system in the composition range  $0.05 \leq x \leq 0.20$  were prepared by using analytically graded  $\text{Bi}(\text{NO}_3)_3 \cdot 5\text{H}_2\text{O}$ ,  $\text{NH}_4\text{VO}_3$ , and  $\text{Pb}(\text{NO}_3)_2$  as

starting materials. Stock solutions of the starting materials (1M) were prepared by dissolving an accurately weighed amount of corresponding material in 50ml deionized water. A 0.2M citric acid used as chelating agent is prepared in deionized water–ethylene glycol mixture at a volumetric ratio of 3:1. A 0.5 M  $\text{NH}_3$  solution is also used for adjusting the pH of sols. The stock solutions of the starting materials were thoroughly mixed at a volumetric ratio of 2:  $x$ : (1– $x$ ) = Bi:Mn:V. Ethylene glycol– citric acid solution was then added to each mixture to form sols, so that the molar ratio of citric acid to total metal ions is maintained at 1.5:1. Under constant stirring,  $\text{NH}_3$  solution is added for adjusting the pH of the sols to ~7. The solution was heated at 80°C with vigorous stirring for one hour to form a transparent gel. The xerogel (precursor metal complex) was then obtained by drying the resulting gel in air at 90°C for 12 hrs. The xerogels were thoroughly mixed in an agate mortar for further homogenization and thereafter calcinated in a muffle furnace at 650°C for 5 hrs. The BIPBVOX powders were pelletized into a cylindrical shape under isostatic pressure of 510 MPa by using Spectralab SL–98. The pellets were then sintered in air at 650°C for 5 hrs.

## 2.2. Structural characterization

X–ray powder diffraction analysis was employed for phase characterization of BIPBVOX system by using Philips PW 1050/30 X–ray diffractometer with  $\text{CuK}\alpha$  radiation ( $\lambda=1.54060 \text{ \AA}$ ). The diffraction beams were collected using the Bragg–Brentano geometry in the range  $10^\circ \leq 2\theta \leq 80^\circ$  with an increment of  $0.018^\circ$  at scan time of 31.16 sec/increment.

Differential Thermal Analysis (DTA) measurements were carried out on Shimadzu SC–TA 60 thermal analyzer. Approximately weighed 20 mg of the dry powder sample was placed in the alumina cell. The experiments were run in  $\text{N}_2$  atmosphere. The flow rate of  $\text{N}_2$  was maintained at  $30 \text{ ml min}^{-1}$  with a heating rate of  $10^\circ\text{C min}^{-1}$  from ambient to 800 °C.

## 2.3. Electrical measurements

AC impedance measurements were carried out on a WayneKerr 4100 LCR meter operated in the frequency range of 50Hz – 1MHz with an AC signal of ~50mV. The sintered pellets were made conducting by applying chemically pure silver paste on both surfaces. The experiments were run in air in the temperature range of 90–650 °C with an increment of 20°C. Impedance spectra were subjected to non–linear least –square fitting using Zview software.

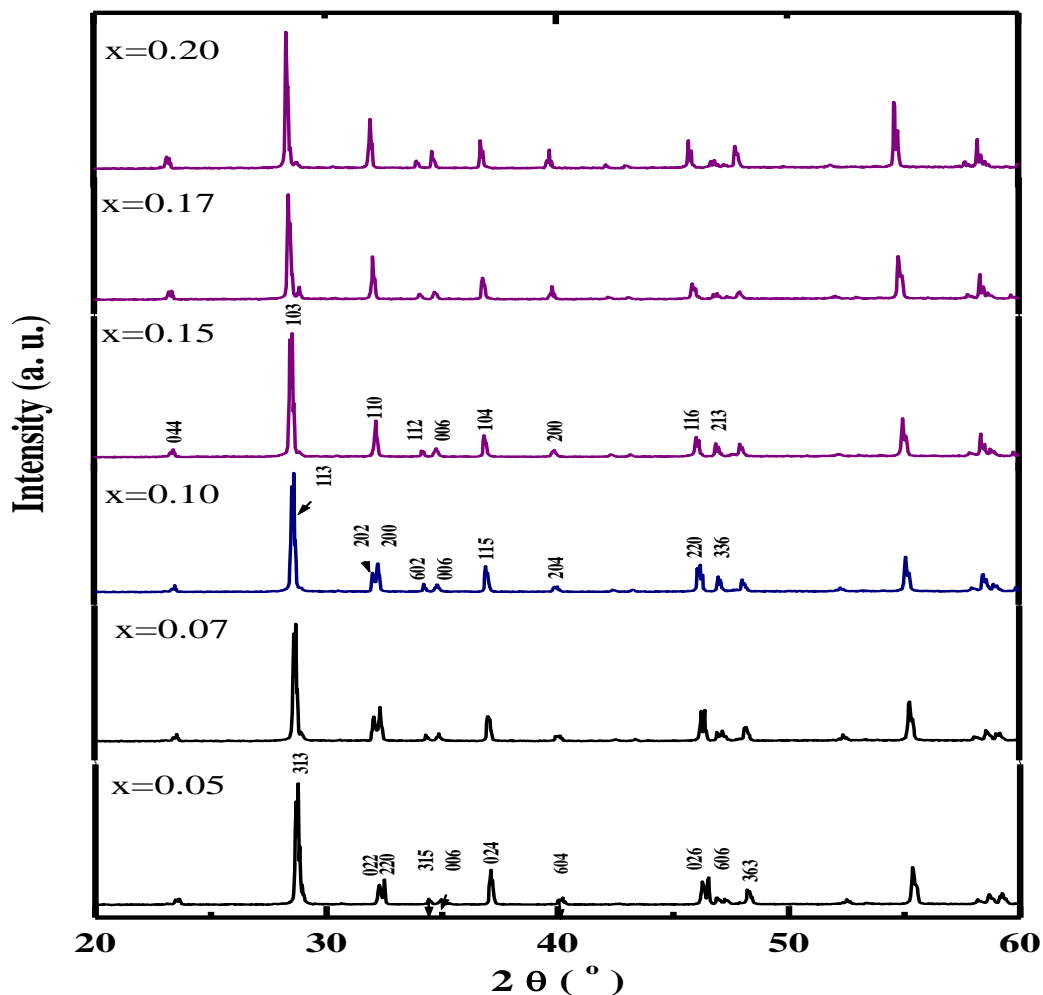
## 2.4. Voltammetric measurements

The high-temperature voltammetric measurements were performed in nitrogen atmosphere containing a small quantity of oxygen on a three-electrode cell of the type: Pt/ $\gamma$ -BIPBVOX. $x$ /YSZ/Pt with the interface Pt/YSZ as a pseudo reference electrode, using a Bipotentiostat (ESA) EI-400. The experimental set-up was made as described by Fafilek et al. [17] and the procedures were thoroughly conducted according to Fafilek and Kurek [14].

## 3. Results and discussion

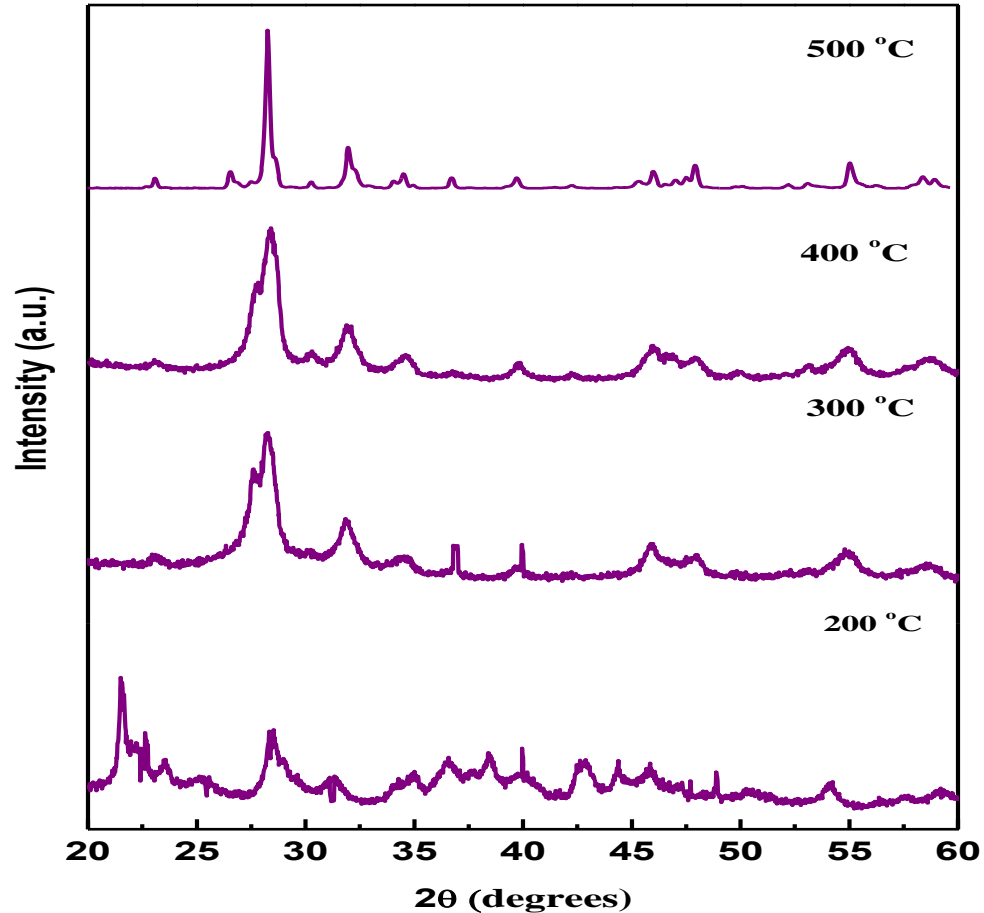
### 3.1. Powder X-ray diffraction

Figure 1 shows the room temperature PXRD patterns of the samples in the composition range  $0.05 \leq x \leq 0.20$  at room temperature. For compositions with  $x \leq 0.07$ , a characteristic doublet is observed between  $2\theta = 46-46.5^\circ$  ascribed to (026), (606) which depicts the presence of monoclinic  $\alpha$  phase as that of the parent compound. For  $x=0.10$ , the doublet merged into a single indexed (220), shows the presence of orthorhombic  $\beta$  phase of higher symmetry. However, the tetragonal  $\gamma$ -phase is stabilized for  $x \geq 0.15$  as clearly evidenced by the presence of a singlet sublattice (110) at  $32.2^\circ$ .



**Figure 1:** PXRD patterns of the BIPBVOX.*x* samples in the composition range  $0.05 \leq x \leq 0.20$ .

Figure 2 depicts the variation in the high temperature PXRD patterns of  $x=0.17$  xerogel as a function of calcination temperature. The sample obtained after calcination at  $400^\circ\text{C}$  for 5 hrs was still found to be somewhat amorphous. At this temperature, the broad diffraction peaks exhibit  $14/mmm$  symmetry, characteristic to the tetragonal phase. However after calcinations to  $500^\circ\text{C}$  the sample was completely converted into a crystalline  $\gamma$ -phase. This can be attributed to the partial decomposition of citrate precursor because in general it was found that the increase in calcination temperature results in the formation of well-crystallized product. It can also be seen that the broadening of the peaks gradually decreases with increasing temperature of the calcination, signifying the increase in crystalline size with increasing temperature [18, 19].



**Figure 2:** PXRD patterns of xerogel with composition  $x=0.17$  calcined at different temperatures.

### 3.2. FT-IR spectra

The above-mentioned results were also confirmed by FT-IR spectra of BIPBVOX. $x$  system shown in Figure 3. It is noticed that with increase in Pb concentration the vibration position of vanadate tetrahedra shifts to lower frequency ( $1031-817\text{ cm}^{-1}$ ). This shift in vanadate tetrahedra can be attributed to the substitution of Pb for V. While the position of Bi-O bands ( $446-429\text{ cm}^{-1}$ ) almost remains similar for all compositions. Moreover, the disappearance of fine structure at  $x=0.20$  in the vanadate anion region reveals the presence of crystallographic disordering in the structure of perovskite layers in the tetragonal phase [20,21].

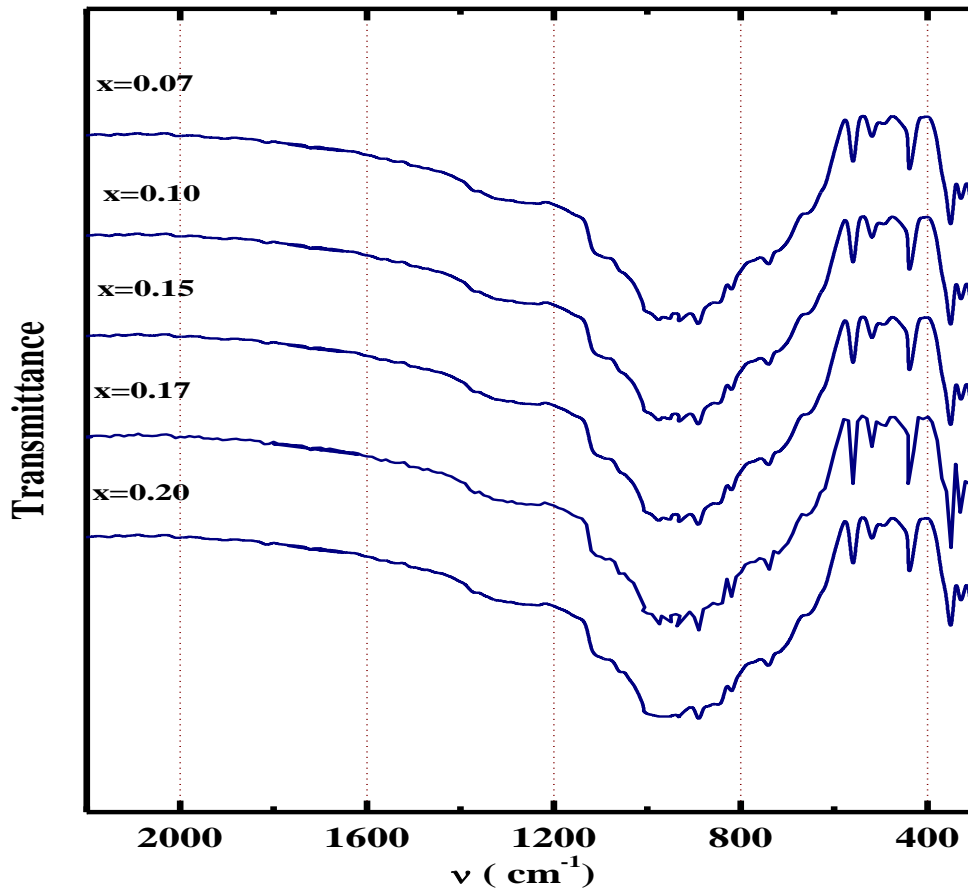


**Figure3:** FT-IR pattern for the BIPBVOX.*x* samples in the composition range  $0.07 \leq x \leq 0.20$ .

Table 1 represents the various IR bands for composition range  $0.07 \leq x \leq 0.20$ . The IR spectrum of the parent compound  $\text{Bi}_4\text{V}_2\text{O}_{11}$  shows bands corresponding to  $\nu_s(\text{V-O})$ ,  $\nu_{as}(\text{V-O})$ ,  $\delta_{as}(\text{O-V-O})$ , modes of vibration assigned to vanadate anion present in  $\alpha\text{-Bi}_4\text{V}_2\text{O}_{11}$  [22]. For  $x=0.07$  and  $x=0.10$ , the IR spectrum seems to imitate the parent compound. Apart from above modes of vibrations, additional bands nearly at  $767\text{--}727\text{ cm}^{-1}$  were observed which are properly assigned to stretching mode of Pb-O band vibrations [20].

**Table1:**FT–IR data for the BIPBVOX.x system.

$x$	$\nu_s (V-O)$ ( $\text{cm}^{-1}$ )	$\nu_{as} (V-O)$ ( $\text{cm}^{-1}$ )	$\delta_{as}(O-V-O)$ ( $\text{cm}^{-1}$ )	$\nu (Bi-O)$ ( $\text{cm}^{-1}$ )	$\nu (Pb-O)$ ( $\text{cm}^{-1}$ )
0 . 0 7	7 4 4	1031,981,882,866	6 5 2	4 4 6	7 2 7
0.10	741	991,923,835	641	443	739
0.15	737	987,886,813	630	437	739
0.17	733	997,864,817	624	446	747
0.20	733	944,817	604	432	767

### 3.3. Differential thermal analysis

The DTA curves of BIPBVOX.xsystem are shown in Figure 4. For  $x=0.07$ , two endothermic peaks observed at  $329^\circ\text{C}$  and  $419^\circ\text{C}$ , depict  $\alpha \leftrightarrow \beta$  and  $\beta \leftrightarrow \gamma$  phase transition, respectively. For  $x=0.10$ , the peak at  $387^\circ\text{C}$  corresponds to  $\beta \leftrightarrow \gamma$  phase transition whereas, the weak endothermic peaks appeared in temperature range  $440 - 520^\circ\text{C}$  for compositions with  $0.15 \leq x \leq 0.20$  show the occurrence of  $\gamma' \leftrightarrow \gamma$  phase transition.

The values of enthalpy ( $\Delta H_t$ ) and onset temperature ( $T_t$ ) of phase transitions as a function of Pb substitution are summarized in Table2. It was found that  $\Delta H_t$  for  $\alpha \leftrightarrow \beta$  transition is larger

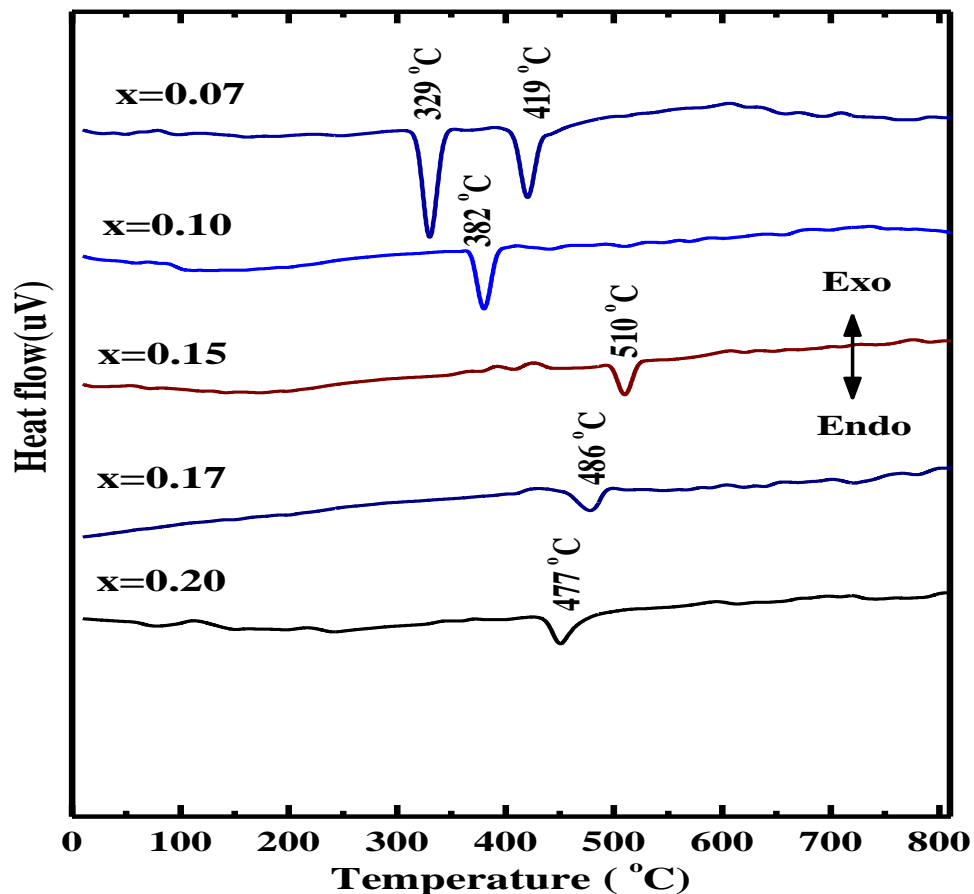


**Figure4:**DTA thermograms of the BIPBVOX.*x*samples versus composition(*x*).

than that required for  $\beta \leftrightarrow \gamma'$  transitions with respect to  $\alpha$ -stabilized phases. Generally, the transition enthalpy and transition temperature decrease with increasing Pb content. This assignment is in a good agreement with the results obtained from the PXR analysis.

### 3.4.AC impedance spectroscopy

Complex plane plots of impedance measured at 350 °C for the BIPBVOX.*x* at various compositions are presented in Figure 5. In all cases, the high- and low-frequency semicircles are respectively assigned to grain and grain boundary contribution to the total electrolyte impedance, while the contribution to impedance of the electrode-electrolyte interface is clearly represented by the inclined spikes appearing at very low frequencies [22].

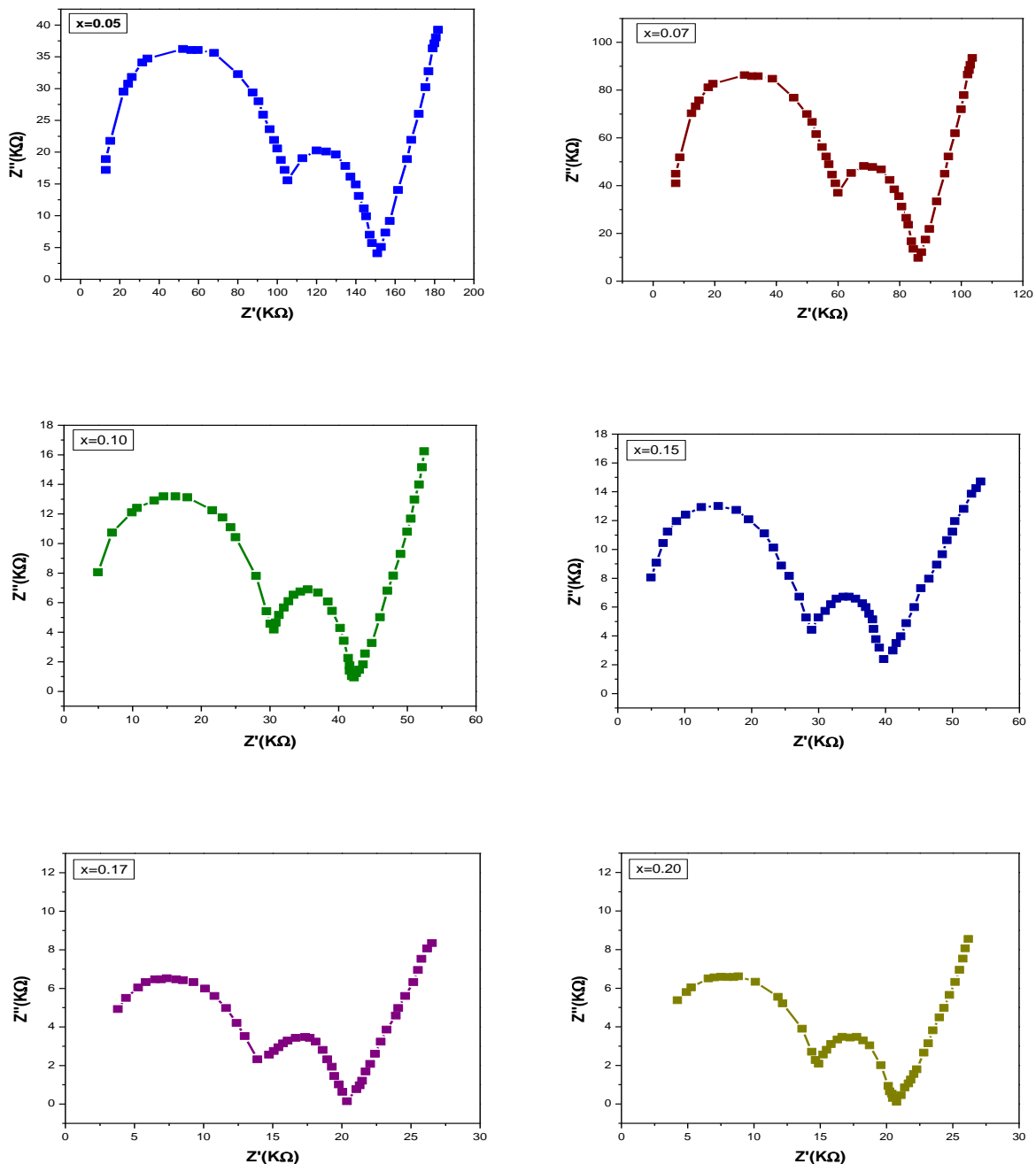


**Figure5:** AC impedance spectra of the BIPBVOX.x system for different compositions measured at 350°C.

The impedance spectra were modeled by an electrical equivalent circuit, comprising of capacitances (C), inductances (L), resistances (R) and constant phase elements (CPE), and were analyzed by means of circular fitting using *Zview* software. More details on deduction and

calculation of equivalent circuit parameters can be found in Ref. [23]. Table 2 summarizes the values of equivalent circuit parameters of both grain and grain boundary contributions which are estimated from the impedance spectra presented in Figure 5. The values of electrolyte resistance are generally reduced as Pb dopant concentration increases. This indicates that the oxide– ion migration within the BIPBVOX crystal is compositionally dependent under isothermal conditions. It can also be noticed that the values of grain resistance ( $R_g$ ) are higher than that of grain boundary resistance ( $R_{gb}$ ) for all compositions at the same measurement temperature, suggesting the major contribution of grain interiors to the overall resistivity of BIPBVOX electrolyte. In contrast, higher values of capacitance are seen at grain boundaries ( $C_{gb}$ ) than that at grain interiors ( $C_g$ ). However, the highest value of  $C_g$  is  $1.50 \times 10^{-9}$  F and of  $C_{gb}$  is  $5.06 \times 10^{-7}$  F found to be for  $x= 0.17$  and  $x= 0.20$ , respectively, revealing a more polarizability of the BIPBVOX solid solution at these limits of Pb substitution [24].

**Table2:** Transition temperatures and enthalpies determined from DTA thermograms.

$x$	$\alpha \leftrightarrow \beta$		$\beta \leftrightarrow \gamma$		$\gamma \leftrightarrow \gamma'$	
	$T_t(^{\circ}\text{C})$	$\Delta H_t(\text{J.g}^{-1})$	$T_t(^{\circ}\text{C})$	$\Delta H_t(\text{J.g}^{-1})$	$T_t(^{\circ}\text{C})$	$\Delta H_t(\text{J.g}^{-1})$
0 . 0 7	3 2 9	8 . 1 1	1 9 5	0		–
0 . 1 0	–	–	3 8 2	4 6		–
0 . 1 5	–	–	–	–	5 1 0	1 5 . 0 7
0 . 1 7	–	–	–	–	4 8 6	1 2 . 2 5
0 . 2 0	–	–	–	–	4 7 7	1 1 . 0 1

### 3.5. Temperature dependence of conductivity

The electrical conductivity of the prepared samples was calculated from the sum of grain and grain boundary resistances, using the relation:

$$\sigma = I/R_t \times (L/A)$$

where  $(L/A)$  is the ratio of thickness to cross section area of the sintered pellet. The temperature dependences of conductivity were computed by using the Arrhenius equation:

$$\sigma T = A \exp(-\Delta E / kT)$$

The Arrhenius plots of conductivity of BIPBVOX system in the composition range  $0.05 \leq x \leq 0.20$  are shown in Figure 6. For compositions  $0.05 \leq x \leq 0.07$ , two line region with different slopes are observed which ascribe to the presence of  $\alpha \leftrightarrow \beta$ , and  $\beta \leftrightarrow \gamma$  phase transition. Whereas the existence of order-disorder  $\gamma' \leftrightarrow \gamma$  phase transition for  $x \geq 0.15$  is confirmed by the existence of single line region with no significant discontinuity between low and high temperature regions. There is merely a point at which activation energy changes. The above results were also previously confirmed by XRD and DTA analysis.

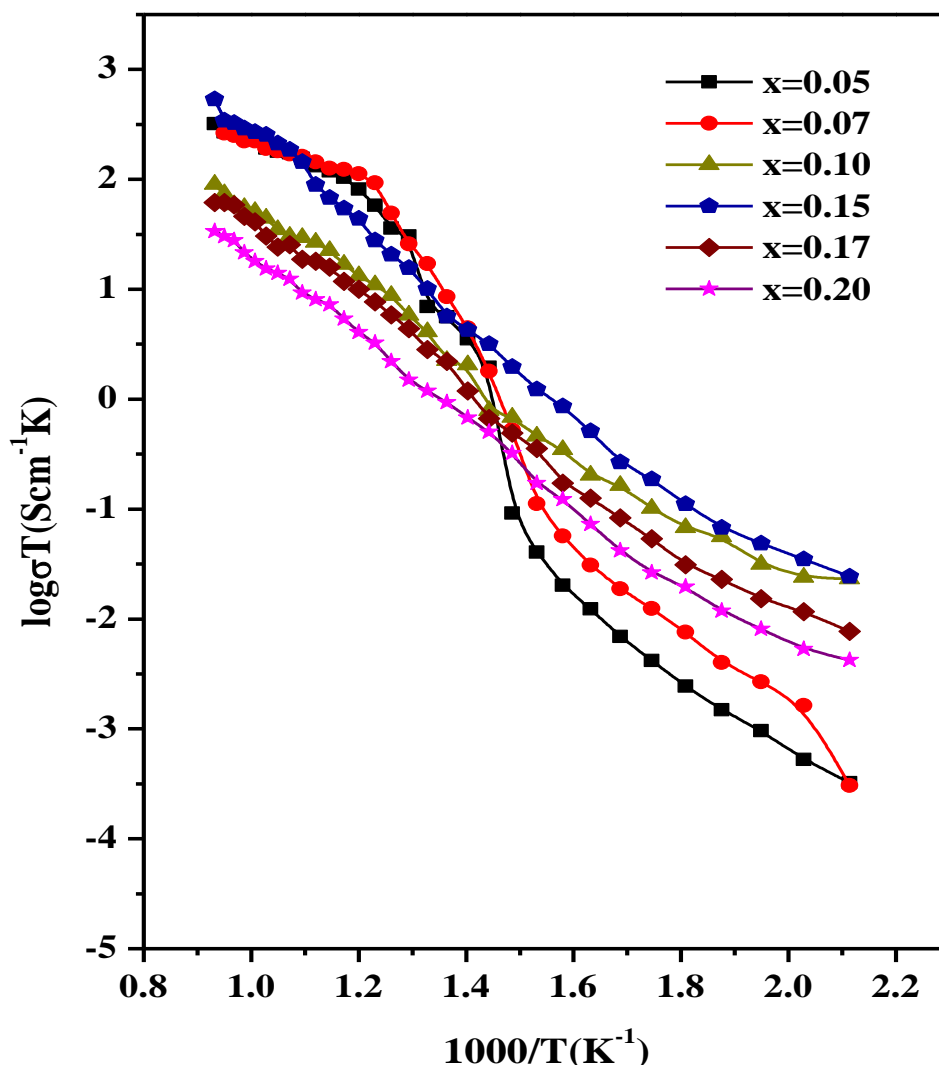


**Figure6:**Arrhenius plots of conductivity on heating for the BIPBVOX.xsamples.

The variation of low temperature conductivity measured at 300 °C ( $\sigma_{300}$ ) and its corresponding activation energy as a function of composition is presented in Figure7a. It is clearly seen that the low temperature conductivity initially increases with a decrease in activation energy as a function of composition up to  $x=0.15$ , where it attains a maximum conductivity of  $6.27 \times 10^{-5} \text{ S.cm}^{-1}$  and thereafter it shows decay. Figure 7b represents the variation in the high-temperature conductivity ( $\sigma_{600}$ ) as a function of lead concentration. It can be noted that the highest value of conductivity ( $0.65 \text{ S.cm}^{-1}$ ) is observed for  $x=0.17$ . Thereafter, the conductivity gradually decreases due to the increase in activation energy.

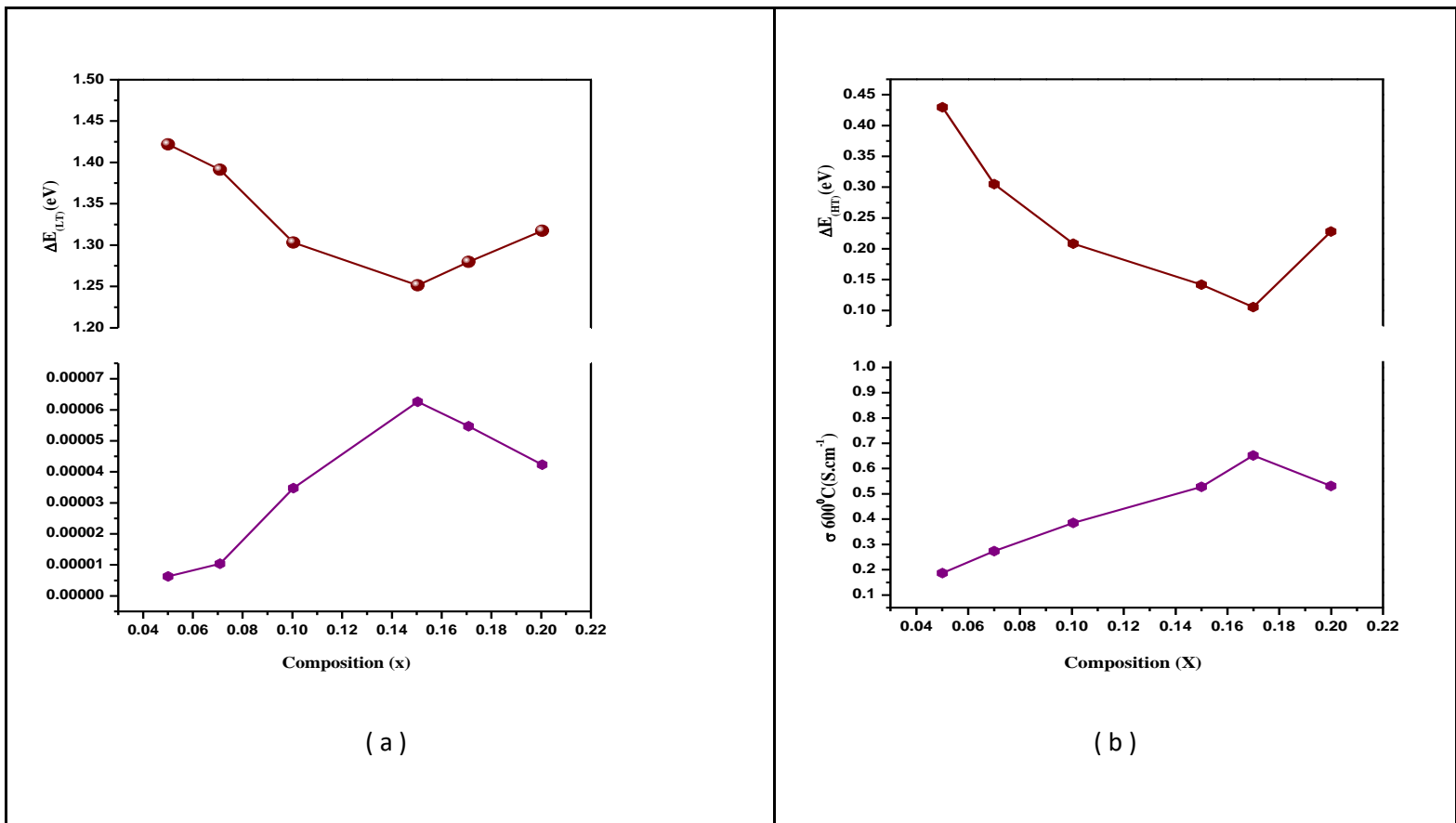
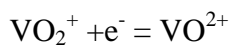


**Figure7:** Variation in the electrical conductivity and corresponding activation energy as a function of composition(x) at lower (a) and higher (b) temperature.

### 3.5. Cyclic voltammetry of $\gamma$ -BIPBVOX.x samples

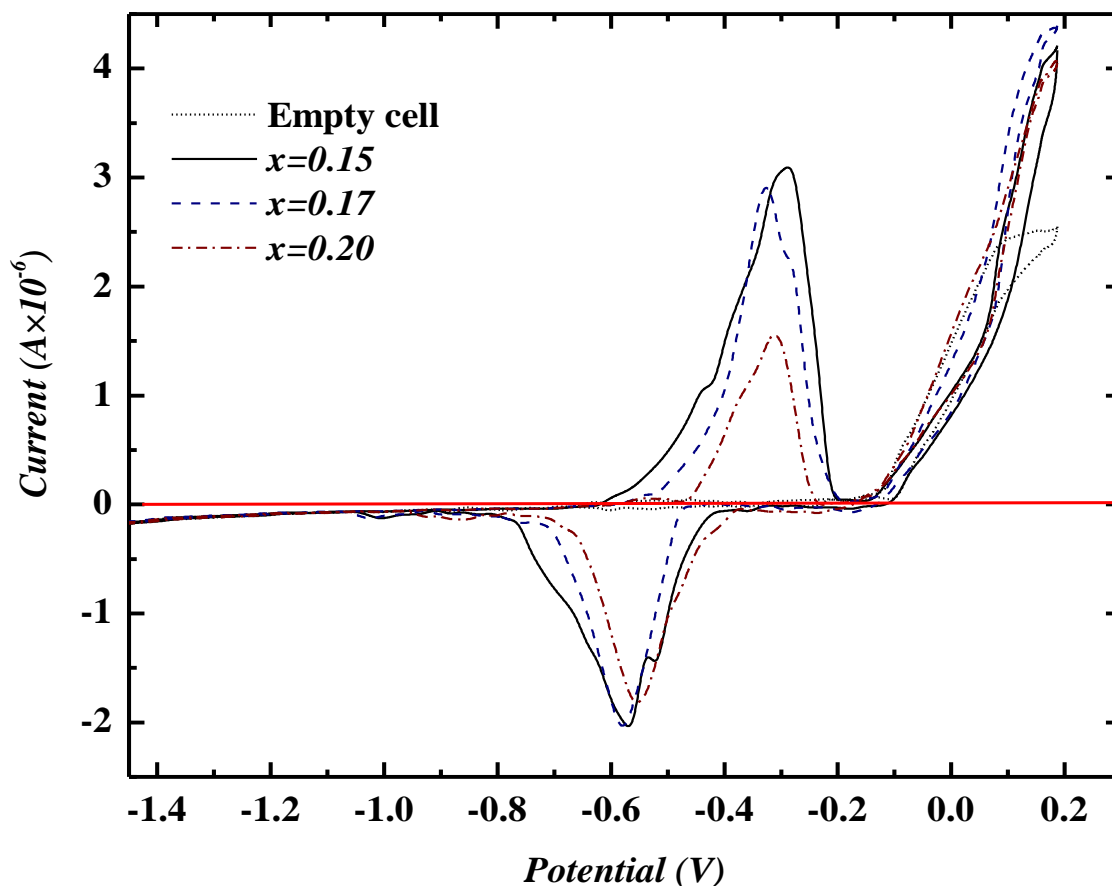
. Cyclic voltammograms of stabilized  $\gamma$ -BIPBVOX.x samples compared to that of the empty cell (Pt/YSZ/Pt) at 300 °C and 600 °C are presented in Figure 8 and 9, respectively. At x=0.15 of 300 °C sintered sample, two potential peaks of forward scan occurred due to the reduction of vanadium and lead [25];



At higher concentration of lead doped samples, results show a slightly shifting of peaks towards more negative values. This observed confluent with disappearing of the lower potential

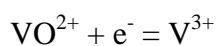
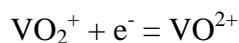
peak, which may referred to the formation of the new composite of lead and vanadium[26-28].

The reverse scan presents the same response of forward peak.



**Figure 8:** Voltammograms of stabilized  $\gamma$ - BIPBVOX phases on the first cycle run in nitrogen atmosphere at 300 °C.

The cyclic voltammogram response of samples sintered at 600°C Fig. 9 introduce four peaks of reduction occurred at  $x=0.15$ , which may attributed to the reduction of lead and vanadium[25];



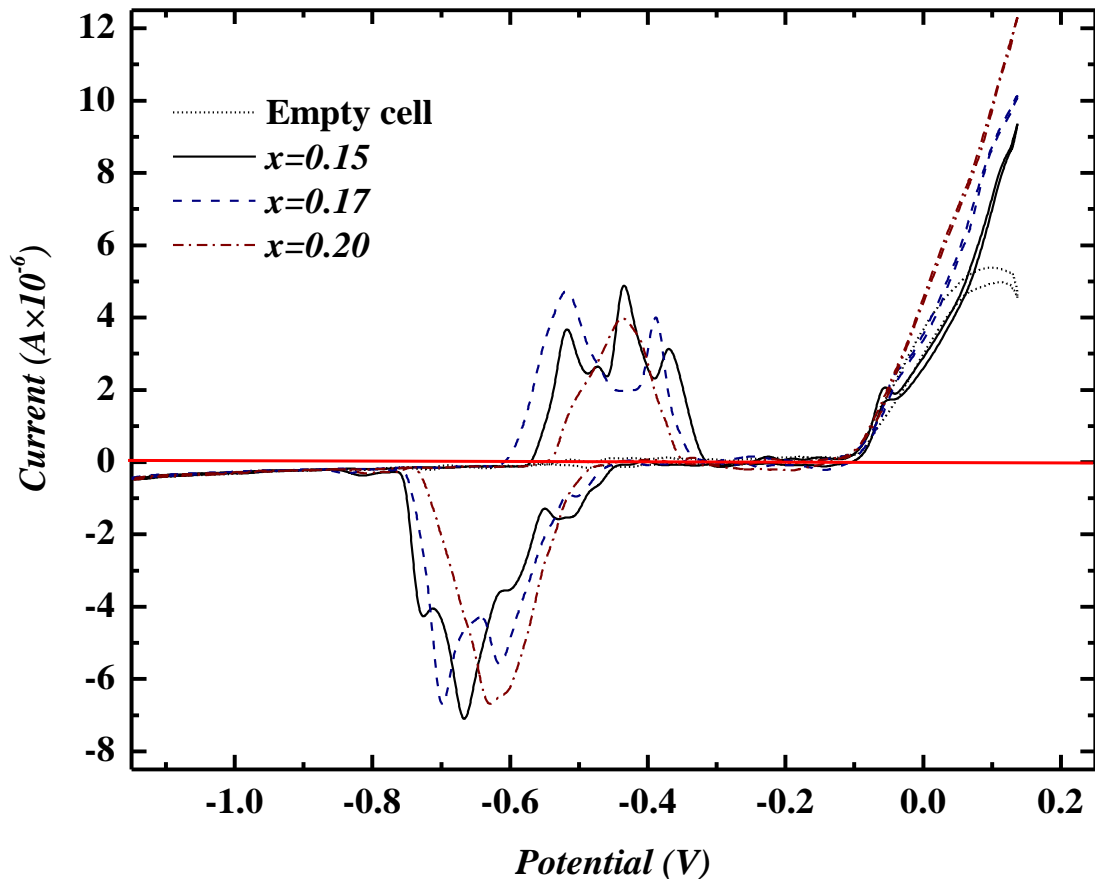


**Figure 9:** Voltammograms of stabilized  $\gamma$ -BIPBVOX phases on the first cycle run in nitrogen atmosphere at 600 °C.

The increasing of lead amount in samples led to disappearing of peaks with broaden of potential response. This overlapping of peaks associated with shifting of reduction potential towards lower values which may attributed to the formation of  $\gamma$ -BIPBVOX. $x$  phase especially for  $x=0.2$  sample where the phase detected clearly by XRD. In the reverse scan, samples introduce a contextually response in the oxidation process.

#### 4. Conclusion

In  $\alpha$ - $\text{Bi}_4\text{V}_2\text{O}_{11}$  single substitution of V by Pb stabilizes the high temperature tetragonal  $\gamma'$ -phase at room temperature for compositions  $x \geq 0.15$ . While the stabilization of orthorhombic  $\beta$ -phase is observed for compositions  $0.10 \leq x < 0.15$ . It was found that the substituted

BIPBVOX. $x$  solid solutions have pronounced ionic conductivity  $6.27 \times 10^{-5} \text{ S.cm}^{-1}$  at  $300^\circ\text{C}$  and  $0.65 \text{ Scm}^{-1}$  at  $600^\circ\text{C}$  for  $x=0.15$  and  $x=0.17$ , respectively. The important point to be emphasized here is that the stability  $\gamma'$ - BIPBVOX. $x$  phases against the reduction of  $\text{Bi}^{3+}$  to metallic bismuth is significantly increased with the increase of Pb dopant concentration. So, these interesting results accordingly confer to the  $\gamma'$ - BIPBVOX. $x$  solid electrolyte a promising application in many of the electrochemical devices operating at moderate temperatures.

## References

- [1] F. Abraham, M.F. Debreuille–Greese, G. Mairesse, and G. Nowogrocki, *Solid State Ionics* 28–30 (1988) 529.
- [2] F. Abraham, J.C. Boivin, G. Mairesse, G. Nowogrocki, *Solid State Ionics* 40–41 (1990) 934.
- [3] J.B. Goodenough, A. Manthiram, M. Paranthaman, Y.S. Zhen, *Mater. Sci. Eng.* B12 (1992) 259.
- [4] C.K. Lee, G.S. Lim, A.R. West, *J. Mater. Chem.* 4 (1994) 1441.
- [5] R.N. Vannier, G. Mairesse, F. Abrahams, G. Nowogrocki, *Solid State Ionics* 80 (1995) 11.
- [6] S. Beg, N.A.S. Al–Arequi, S. Haneef, *Solid State Ionics* 179 (2008) 2260.
- [7] N.S.A. Al–Arequi, S. Beg, A. Al–Alas, *J. Phys. Chem. Solids* 73(2012)730.
- [8] S. Beg, N. A. S. Al–Arequi, A. Al–Alas, S. Hafeez, *Ionics* 20 (2014) 269.
- [9] C. Pirovano, M. C. Steil, E. Capoen, G. Nowogrocki, R.N. Vannier, *Solid State Ionics* 176 (2005) 2079.
- [10] J.R. Dygas, M. Malys, F. Krok, W. Wrobel, A. Kozanecka, and I. Abrahams, *Solid State Ionics* 176 (2005) 2085.
- [11] S. Beg, S. Hafeez, N. A.S. Al–Arequi, *Solid State Ionics* 261 (2014) 125.
- [12] T. Iharada, A. Hammouche, J. Fouletier, M. Kleitz, J.C. Bovin, G. Mairesse, *Solid State Ionics* 48 (1991) 257.
- [13] G. Fafilek, *Solid State Ionics* 113–115 (1998) 623.
- [14] G. Fafilek and P. Kurek, *Solid State Ionics* 136–137 (2000) 67.
- [15] G. Fafilek, S. Harasek, *Solid State Ionics* 119 (1999) 91.
- [16] J. Yan, M. Greenblatt, *Solid State Ionics* 81(1995) 225.
- [17] G. Fafilek, K. Leeb, M.W. Breiter, *Solid State Ionics* 86–88(1996) 1415.
- [18] R.A. Rocha, E.N.S. Muccillo, *Mater. Res. Bull.* 38 (2003) 1979.
- [19] S. Beg, A. Al–Alas, N.A.S. Al–Arequi, *J. Alloys Comps* 504 (2010) 413.
- [20] K. Nakamoto, *Infrared and Raman Spectra of Inorganic and Coordination Compounds*, Wiley, New York, 1997.
- [21] V.P. Tolstoy, E.V. Tolstobrov, *Solid State Ionics* 151(2002)165.
- [22] M. Guillodo, J. Fouletier, L. Dessemond, P.D. Gallo, *J. Eur. Ceram. Soc.* 21 (2001) 2331.
- [23] A. Al–Alas, S. Beg, N. A. S. Al–Arequi, S. Hafeez, *J. Eur. Ceram. Soc.* 33 (2013) 2111.
- [24] A. Kezionis, W. Bogusz, F. Krok, J. Dygas, A. Orliukas, I. Abrahams, W. Gebicki, *Solid State Ionics* 119 (1999) 145.

- [25]D.R. Lide, ed., CRC Handbook of Chemistry and Physics, 90th Edition, (CD-ROM version 2010), CRC Press, Taylor and Francis, Boca Raton, FL.
- [26]T.Grygar,F.Marken,U.Schröder,andF.Scholz,ChemInformAbstract:ElectrochemicalAnalysis ofSolids.AReview.*ChemInform*,2002.33(27)
- [27]B.Centeno,M.L.Tascón,M.D.Vázquez,andP.SánchezBatanero,ElectrochemicalstudyofPbO<sub>2</sub>at a carbon paste electrode with electrolytic binder.*ElectrochimicaActa*,1991.36(2)
- [28]P.T.Kissinger,andW.R.Heineman,Cyclic voltammetry.*Journal of Chemical Education*,1983.60 (9)